Atmos. Chem. Phys., 16, 5745–5761, 2016
www.atmos-chem-phys.net/16/5745/2016/
doi:10.5194/acp-16-5745-2016

Atmospheric Chemistry and Physics Open Access EGU

Air–sea fluxes of CO_2 and CH_4 from the Penlee Point Atmospheric Observatory on the south-west coast of the UK

Mingxi Yang[1], Thomas G. Bell[1], Frances E. Hopkins[1], Vassilis Kitidis[1], Pierre W. Cazenave[1], Philip D. Nightingale[1], Margaret J. Yelland[2], Robin W. Pascal[2], John Prytherch[3], Ian M. Brooks[3], and Timothy J. Smyth[1]

[1]Plymouth Marine Laboratory, Prospect Place, Plymouth, PL1 3DH, UK
[2]National Oceanography Centre, European Way, Southampton, SO14 3ZH, UK
[3]Institute for Climate and Atmospheric Science, School of Earth and Environment, University of Leeds, Leeds, UK

Correspondence to: Mingxi Yang (reelguy@gmail.com)

Received: 15 September 2015 – Published in Atmos. Chem. Phys. Discuss.: 18 January 2016
Revised: 18 April 2016 – Accepted: 21 April 2016 – Published: 11 May 2016

Abstract. We present air–sea fluxes of carbon dioxide (CO_2), methane (CH_4), momentum, and sensible heat measured by the eddy covariance method from the recently established Penlee Point Atmospheric Observatory (PPAO) on the south-west coast of the United Kingdom. Measurements from the south-westerly direction (open water sector) were made at three different sampling heights (approximately 15, 18, and 27 m above mean sea level, a.m.s.l.), each from a different period during 2014–2015. At sampling heights ≥ 18 m a.m.s.l., measured fluxes of momentum and sensible heat demonstrate reasonable ($\leq \pm 20$ % in the mean) agreement with transfer rates over the open ocean. This confirms the suitability of PPAO for air–sea exchange measurements in shelf regions. Covariance air–sea CO_2 fluxes demonstrate high temporal variability. Air-to-sea transport of CO_2 declined from spring to summer in both years, coinciding with the breakdown of the spring phytoplankton bloom. We report, to the best of our knowledge, the first successful eddy covariance measurements of CH_4 emissions from a marine environment. Higher sea-to-air CH_4 fluxes were observed during rising tides (20 ± 3; 38 ± 3; 29 ± 6 µmole m^{-2} d^{-1} at 15, 18, 27 m a.m.s.l.) than during falling tides (14 ± 2; 22 ± 2; 21 ± 5 µmole m^{-2} d^{-1}), consistent with an elevated CH_4 source from an estuarine outflow driven by local tidal circulation. These fluxes are a few times higher than the predicted CH_4 emissions over the open ocean and are significantly lower than estimates from other aquatic CH_4 hotspots (e.g. polar regions, freshwater). Finally, we found the detection limit of the air–sea CH_4 flux by eddy covariance to be 20 µmole m^{-2} d^{-1} over hourly timescales (4 µmole m^{-2} d^{-1} over 24 h).

1 Introduction

Carbon dioxide (CO_2) and methane (CH_4) are two of the most important greenhouse gases in the earth's atmosphere. Over the last few decades, large efforts have gone into quantifying the impact of the ocean on the CO_2 and CH_4 budgets. Air–sea fluxes of these gases are usually estimated via a "bulk" formula, i.e. as the product of the waterside gas transfer velocity k_W and the air–sea concentration difference. Globally, the open ocean takes up approximately a quarter of the anthropogenic CO_2 emissions (Le Quéré et al., 2015). This estimate, limited in accuracy partly by uncertainties in k_W, is used in global models to constrain the terrestrial CO_2 uptake (e.g. Manning and Keeling, 2006; Canadell et al., 2007).

The shelf seas make up only a small fraction of the global oceans, but support a significant portion of global primary productivity and draw a substantial flux of atmospheric CO_2 into the ocean (Chen et al., 2013). Muller-Karger et al. (2005) estimated that the shelf seas might be responsible for as much as 40 % of global oceanic carbon sequestration. The majority of the atmospheric CO_2 taken up by European shelf seas is subsequently exported into the Atlantic Ocean (Thomas et al., 2004). Compared to the open ocean, the coastal zone tends to be more spatially and temporally heterogeneous, increasing the uncertainty in carbon flux estimates. Regions

influenced by riverine outflow and anthropogenic activities can be net sources or sinks of atmospheric CO_2 (Chen et al., 2013). Processes such as respiration of allochthonous (terrestrial) organic carbon inputs, benthic–pelagic coupling, variability in surfactant abundance, and near-surface stratification are likely to have greater importance in shallow waters. Furthermore, k_W derived from the open ocean may not always be applicable to shallow waters, where waves shoal and break more frequently, and tidal flow and currents could become more important (e.g. Upstill-Goddard, 2006). Monitoring of CO_2 fluxes in such dynamic and variable environments necessitates a continuous, high temporal resolution methodology (Edson et al., 2008), such as the eddy covariance (EC) technique.

Based on seawater CH_4 concentrations and global modelling, CH_4 emission from the open ocean to the atmosphere has been estimated to be 0.4–18 Tg yr^{-1}, an uncertain but probably small term in the global CH_4 budget (Bates et al., 1996; Bange et al., 1994; Lelieveld et al., 1998). In certain regions such as the Arctic, however, ice melt can expose underlying CH_4-rich waters (e.g. Shakhova et al., 2010; Kitidis et al., 2010). Enhanced mixing ratios of CH_4 were measured on low-elevation flights over regions of fractional ice cover and open leads in the Arctic, suggesting a large surface source (Kort et al., 2012). On a per area basis, shelf seas, rivers, and estuaries tend to have much greater CH_4 emissions than the open ocean due to benthic methanogenesis (Bange, 2006; Upstill-Goddard et al., 2000; Middelburg et al., 2002). Global CH_4 emissions from coastal regions are poorly quantified and may be influenced by processes such as riverine outflow and tidal circulations. In shallow waters, ebullition (bubbles rising from the sediment) represents an additional pathway for CH_4 transfer (Dimitrov, 2002; Kitidis et al., 2007). Some bubbles are not fully dissolved in seawater before surfacing and this transfer to the atmosphere is not accounted for in bulk flux calculations based on aqueous CH_4 concentrations.

Direct air–sea flux measurements would help to constrain CH_4 cycling and could also improve our understanding of the physical processes that drive gas transfer. Thus far, estimates of k_W from sparingly soluble gases such as CO_2 and $^3He/SF_6$ (e.g. Sweeney et al., 2007; McGillis et al., 2001; Nightingale et al., 2000) increase more rapidly with wind speed than those derived from the more soluble dimethyl sulfide (e.g. Huebert et al., 2004; Yang et al., 2011; Bell et al., 2013). This divergence may be due to bubble-mediated gas exchange resulting from breaking waves (Blomquist et al., 2006). CH_4 is much less soluble than CO_2 in seawater and should thus be transferred even more efficiently by bubbles.

We measured air–sea CO_2, CH_4, momentum, and sensible heat fluxes by the EC method at the Penlee Point Atmospheric Observatory (PPAO) during three periods at three sampling heights: May–June 2014 ($\sim$ 15 m above mean sea level, a.m.s.l.), June–July 2014 ($\sim$ 27 m), and April–June 2015 ($\sim$ 18 m). The influences of sampling height and wind direction on fluxes are examined in Sect. 3.2. To evaluate how representative our measurements are of air–sea transfer, EC fluxes of momentum and sensible heat are compared to open-ocean bulk formulae based on mean wind speed and air/sea temperatures (Sect. 3.3). We illustrate wind direction and diel variations in atmospheric CO_2 and CH_4 mixing ratios (Sect. 4.1). Marine CH_4 emissions have not been quantified previously by EC and here we estimate the detection limit of this measurement (Sect. 4.2). Focusing on the open water wind sector, we elucidate the drivers for the variability in CO_2 and CH_4 fluxes (Sects. 4.3 and 4.4).

2 Experimentation

2.1 Environmental setting

The Penlee Point Atmospheric Observatory (50°19.08′ N, 4°11.35′ W; http://www.westernchannelobservatory.org.uk/penlee/) was established in May 2014 by the Plymouth Marine Laboratory (PML) on the south-west coast of the United Kingdom for long-term observations of air–sea exchange and atmospheric chemistry. PPAO is in close proximity to two nearby long-term marine stations that form the Western Channel Observatory (http://www.westernchannelobservatory.org.uk). Meteorological variables (wind, temperature, humidity, and pressure), sea surface temperature (SST), salinity, chlorophyll, oxygen, and dissolved organic matter are measured continuously from buoys stationed at L4 (50°15.0′ N, 4°13.0′ W) and E1 (50°02.6′ N, 4°22.5′ W), which are about 6 and 18 km south of PPAO. Seawater pCO_2 is measured on weekly cruises to the L4 station and biweekly cruises to the E1 station (Kitidis et al., 2012).

PPAO is situated on an exposed headland on the western edge of the Plymouth Sound, which is primarily fed by the Tamar Estuary from the north-west and is open to the Atlantic Ocean to the south-west (Fig. 1). South-south-west of PPAO, the water depths increase steadily to $\sim$ 8, 15, 22, and 24 m (relative to mean sea level) at horizontal distances of 100, 300, 1000, and 1300 m (www.channelcoast.org). Northeasterly wind comes over the Plymouth Sound to PPAO and is limited to a fetch of about 5 km. Air from the southeast is affected by pollution from the European continent as well as shipping emissions (Yang et al., 2016). In the southwesterly direction, the wind fetch is up to thousands of km and the wind speed sometimes exceeds 20 m s^{-1}. This brings in air that has much less anthropogenic influence and is more representative of the background Atlantic atmosphere (see Sect. 4.1).

The stone PPAO building (length, width, height of 3.5, 3.5, 3.0 m) is approximately 11 m a.m.s.l., mains powered, vehicle-accessible, and uses line-of-sight radioethernet to communicate with PML (6 km to the north-north-east). A small strip of land and a narrow, rocky intertidal zone sep-

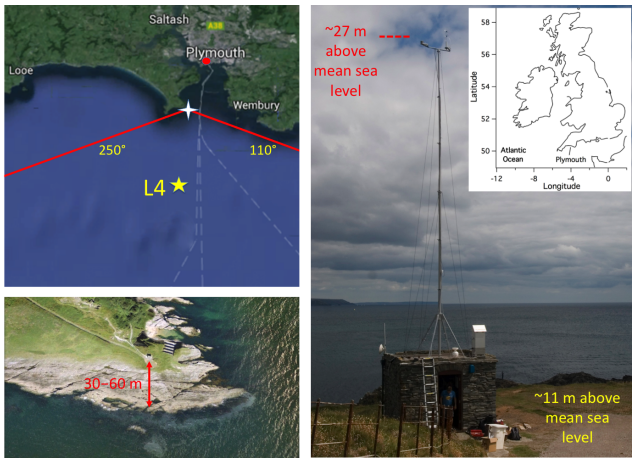

Figure 1. Top left: location of the Penlee Point Atmospheric Observatory (white cross). PPAO is ∼ 6 km south-south-west of the Plymouth Marine Laboratory (red dot), ∼ 6 km north of the L4 station (yellow star), and ∼ 18 km north of the E1 station (beyond the southerly extent of the map). White dashed lines are commercial ferry routes. Bottom left: a close up map showing the foreshore around the PPAO hut. Right: PPAO with the telescopic mast fully raised. North is up in both maps on the left.

arate the building from the sea. South-west and north-east of PPAO, the horizontal distance to the water's edge is 30–60 m, depending on the tide. South-east of PPAO, the distance to water is greater (about 70–90 m) due to an exposed rocky outcrop. The local tidal amplitudes (semi-diurnal) are ∼ 5 m during spring tide and ∼ 2 m during neap tide. The intertidal zone is only sparsely covered by macroalgae (< 10 % by area), likely due to frequent exposure to large waves.

2.2 Turbulent flux instrumentation

During May–June 2014, a sonic anemometer (Gill Windmaster Pro) and a meteorology station (Gill Metpak Pro) were mounted on a metal pole about 1.4 m above the PPAO rooftop. A telescopic mast (retracted length of 2.8 m and fully extended length of 12.3 m; Clark Masts) was installed on top of the observatory roof (Fig. 1) on 17 June 2014. The Windmaster Pro anemometer and the meteorology station were then moved to a cross bar on top of the mast. In February 2015, another sonic anemometer (Gill R3) was installed at the same height as the Windmaster Pro, about 80 cm apart in the horizontal. The sonic anemometers measure 3-dimensional wind velocities (u, v: the two horizontal components; w: the vertical component) at 10 Hz (Windmaster Pro) and 20 Hz (R3). Table 1 summarises measurement periods and corresponding sensor heights.

We deployed the Windmaster Pro and the R3 sonic anemometers side by side for two reasons. First, signal dropouts at high frequencies were common for the Windmaster Pro during moderate-to-heavy precipitation, which tended to coincide with strong south-westerly winds. Valid flux measurements from the Windmaster Pro, limited to mostly dry periods, may thus be biased towards low-to-intermediate wind speeds. Second, initial drag coefficient measurements from the Windmaster Pro at PPAO were lower than expected compared to published results for air–sea momentum flux. The manufacturer Gill report a firmware bug in the Windmaster Pro and recommend a bias correction to the w axis (+16.6 % for positive w; 28.9 % for negative w; see technical key note: http://gillinstruments.com/data/manuals/KN1509_WindMaster_WBug_info.pdf). This correction is not necessary for the R3 anemometer, which has individually calibrated u, v, and w components. Simultaneous deployments of these two anemometers allow us to evaluate the effectiveness of the Windmaster Pro correction (Sect. 3.3).

2.3 CO_2 and CH_4 measurements

Atmospheric mixing ratios of CO_2 and CH_4 were measured by a Picarro cavity-ringdown analyzer (G2311-f) at a frequency of 10 Hz (flux mode). The inlet to this analyzer was mounted ∼ 30 cm below the centre volume of the Windmaster Pro anemometer. An external dry vacuum pump drew sample air via a ∼ 18 m long, 3/8″ OD Teflon perfluoroalkoxy (PFA) tubing at a flow rate of initially ∼ 30 L min^{-1}. The pump performance deteriorated over time due to constant exposure to sea salt. A high-performance particulate arrestance (HEPA) filter was installed immediately upstream of the pump in late 2014, which resulted in a ∼ 15 L min^{-1} reduction of the main flow. The Picarro instrument subsampled from the main flow via a ∼ 2 m long, 1/4″ OD Teflon PFA tubing at a rate of ∼ 5 L min^{-1}. Airflow was fully turbulent throughout the inlet.

The presence of water vapour (H_2O) degrades the measurements of CO_2 and CH_4 via dilution, spectral interference and line broadening (Rella, 2010). Miller et al. (2010) and Blomquist et al. (2014) found that ambient variability in H_2O mixing ratio causes significant bias to the EC measurements of air–sea CO_2 flux. We followed the recommendation of Blomquist et al. (2014) and dried the sampled air using a high-throughput dryer (Nafion PD-200T-24M). H_2O efficiently permeates through the Nafion membrane while CO_2 and CH_4 essentially do not. Set up in counter-flow mode (reflux configuration), the dryer utilises the lower pressure of the Picarro exhaust air to dry the sample air. The ambient H_2O mixing ratio is typically on the order of 1 % at PPAO. With the dryer inline the measured H_2O mixing ratio was reduced by 5 to 10-fold. The Picarro instrument reports mixing ratios of CO_2 and CH_4 in sample air based on precisely controlled cavity temperature and pressure. An internal, point-by-point correction by the instrument for residual humidity yields the dry mixing ratios (C_{CO_2} and C_{CH_4}), which we use for flux computations. Air density fluctuations (i.e. Webb et al., 1980) should thus not affect our measurements. Tuned by the manufacturer prior to our first use, we checked the instrument calibration with CO_2 and CH_4 gas standards (BOC) and

Table 1. Summary of sampling periods, mast height above observatory rooftop and above mean sea level (a.m.s.l.), and hourly eddy covariance CH_4 fluxes (μmole m^{-2} d^{-1}) for the south-west wind sector (180–240°). CH_4 fluxes when the sampling height was 15 m a.m.s.l. are likely to be underestimates of air–sea transfer because a significant portion of the flux footprint was over land (Sect. 3). For the last period (2015), fluxes are computed from both the Windmaster Pro and R3 sonic anemometer (shown in that order). SE indicates standard error.

	Sensor height (m)		EC flux	Falling tide	Rising tide
Time	Over roof	a.m.s.l.	Mean (SE)	Mean (SE)	Mean (SE)
14 May – 17 June 2014	1.4	∼ 15	16 (2)	14 (2)	20 (3)
17 June – 21 July 2014	13.3	∼ 27	24 (4)	21 (5)	29 (6)
21 April – 3 June 2015	3.6	∼ 18	25 (2), 30 (2)	19 (2), 22 (2)	33 (3), 38 (3)

occasionally determined the instrument backgrounds with nitrogen gas. CO_2 and CH_4 measurements were unavailable between August 2014 and March 2015 due to faults in the Picarro instrument.

3 Suitability of the site for air–sea transfer measurements

3.1 Eddy covariance flux processing

In the eddy covariance method, flux is determined from the correlation between the vertical wind velocity (w) and the variable of interest (x): $\overline{w'x'}$. Here the primes indicate fluctuations from the means while the overbar denotes temporal averaging. The coastal environment near PPAO is complex and heterogeneous in both air and water phases. Shifts in air mass and wind direction result in substantial changes in air temperature and gas-mixing ratios. Thus we chose a relatively short averaging interval of 10 min (as used by e.g. Miller et al., 2010) to more easily satisfy the homogeneity/stationarity requirements for eddy covariance (see Appendix A for flux quality control).

For the computations of CO_2 and CH_4 fluxes ($\overline{w'C_{CO_2}'}$, $\overline{w'C_{CH_4}'}$), an lag correlation analysis is performed hourly to determine the time delay between the instantaneous vertical winds and gas-mixing ratio measurements. Most of the atmospheric variability in CO_2 and CH_4 is caused by horizontal transport rather than the air–sea flux. Detrending the gas-mixing ratios to remove low-frequency variability improves the accuracy of the lag-time determination. Between May and July 2014, a delay of 1.9 ± 0.1 s was found between w (Windmaster Pro anemometer) and C_{CO_2}. After the installation of the HEPA filter, the delay increased to 3.3 ± 0.1 s. Lag times derived from w and C_{CH_4} are much noisier due to the smaller magnitude of the CH_4 flux. We apply the lag correction determined from the $w : C_{CO_2}$ analysis to the CH_4 flux calculation. Ten-minute segments of CO_2 and CH_4 fluxes that pass the quality control criteria (see Appendix A) are further averaged to hourly intervals, which reduces random noise by a factor of $\sim N^{0.5}$, where N is the number of valid flux segments. Only hours with at least three 10 min flux intervals are considered for further analysis.

3.2 Evaluation of wind sectors

A double rotation (Tanner and Thurtell, 1969; Hyson et al., 1977) streamline correction is applied to wind data in 10 min blocks prior to flux computation. Tilt angles between the horizontal and vertical planes from this calculation for sampling heights of 15, 18, and 27 m a.m.s.l. are shown in Fig. 2. During onshore airflow, the mean tilt angle is positive as air is forced upwards. The magnitude of this tilt for the south-westerly wind, which blows perpendicularly across the Penlee headland and makes contact with water again to the north-east, is comparable to shipboard measurements. The tilt angle is negative in the north-west sector due to the presence of a small hill behind the observatory building in that direction. A comparison of horizontal wind speed between Penlee and the L4 buoy when the wind is from the south-west does not show, within measurement uncertainties, a significant acceleration in the Penlee measurement (e.g. as might be expected when air is forced over a large superstructure). Thus the hill to the north-west of the site should not have a major influence on our measurements during south-westerly conditions. A peak in tilt angle near 120°, more apparent at low sampling heights, is likely caused by the exposed rocky outcrop in that direction. The impact of this local topography is reduced with increasing sampling height.

From the friction velocity $u_* = (\overline{u'w'}^2 + \overline{v'w'}^2)^{1/4}$ and wind speed (U_{true}), we compute the drag coefficient $C_D = (u_*/U_{true})^2$. Bin-averaged C_D at the three sampling heights as a function of wind direction is shown in Fig. 3. At 15 and 18 m a.m.s.l., measured C_D from about 80 to 150° are clearly elevated compared to open-ocean values (which typically range between 0.5×10^{-3} and 2.5×10^{-3} depending on the wind speed; Edson et al., 2013). This is likely because a part of the flux footprint overlapped with the rocky outcrop in that direction, which has a greater roughness length than the surface ocean. Likewise, high C_D values between 250 and 40° are caused by land. The impact from the rocky outcrop to the south-east is no longer obvious at a sampling height

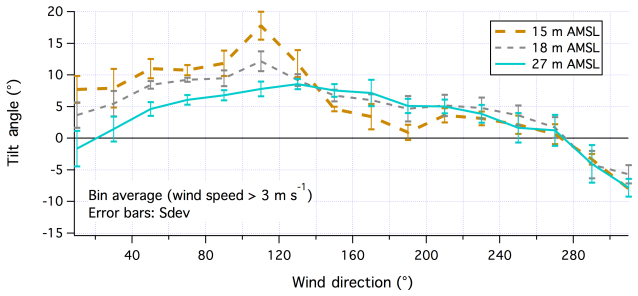

Figure 2. Tilt angle vs. true wind direction at three sampling heights. Lines represent averages (wind speed $> 3\,\mathrm{m\,s^{-1}}$ only) and the error bars indicate standard deviations within each wind direction bin. Wind data are from the Windmaster Pro sonic anemometer.

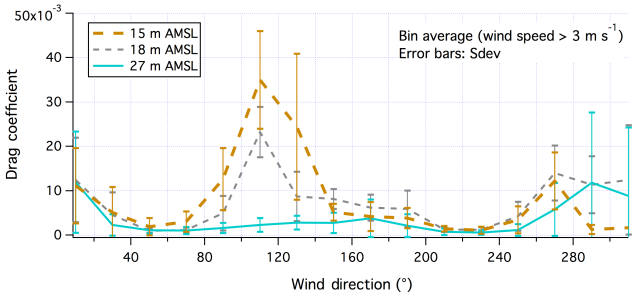

Figure 3. Drag coefficient vs. true wind direction at three sampling heights. Lines represent averages (wind speed $> 3\,\mathrm{m\,s^{-1}}$ only) and the error bars indicate standard deviations within each wind direction bin. Wind data are from the Windmaster Pro sonic anemometer.

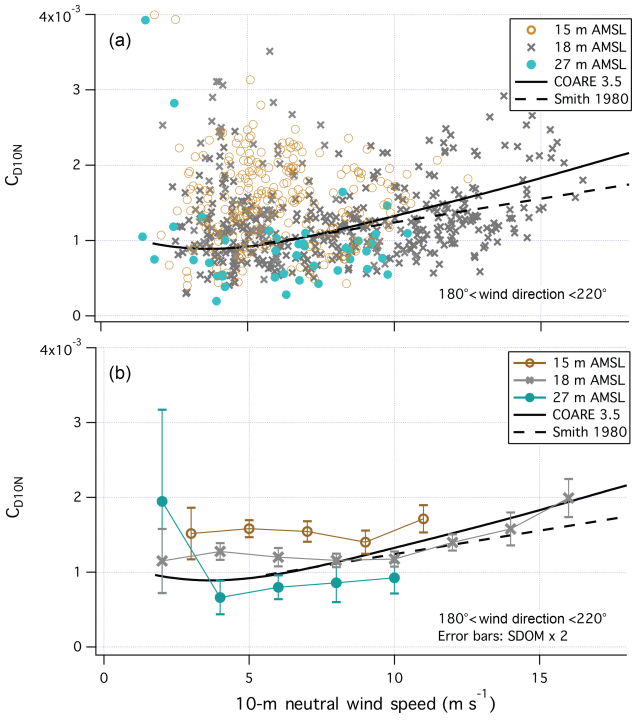

Figure 4. 10 m neutral drag coefficient vs. 10 m neutral wind speed at sampling heights of 15, 18, and 27 m a.m.s.l. **(a)** 10 min EC measurements, **(b)** bin averages, with error bars indicating two standard errors within each wind speed bin. Wind data are from the Windmaster Pro sonic anemometer. Also shown are C_{D10N} parameterized from the COARE model version 3.5 (Edson et al., 2013) and Smith (1980).

of 27 m a.m.s.l., when the flux footprint shifts further away from the observatory. For winds blowing from the north-east and south-west, measured C_{D} is lower and much closer to values expected for the open ocean. North-easterly winds are relatively infrequent ($\sim 8\,\%$ of the time) and limited in fetch; also the air mass from that direction is affected by terrestrial pollution and ship emissions. We thus focus on the more frequent ($\sim 20\,\%$ of the time) south-west wind sector (180–240°) for most of this paper. In Appendix B, we compute the theoretical flux footprints at different sampling heights and during various atmospheric conditions/tidal cycles. For south-westerly winds, land influence is predicted to be only a few percent when the mast height is ≥ 18 m a.m.s.l.

3.3 Verification of momentum and sensible heat transfer

Here we compare the 10-m neutral drag coefficient ($C_{\mathrm{D10N}=(u_*/U_{10\mathrm{N}})^2}$) and sensible heat fluxes to the fairly well established open-ocean bulk formulae predictions. The 10-m neutral wind speed $U_{10\mathrm{N}}$ is determined using Businger–Dyer relationships (Businger, 1988) from the wind speed and air temperature at PPAO, tidal-dependent sampling height, and SST from L4. EC sensible heat flux is derived from the sonic temperature and further corrected for humidity using the bulk latent heat flux. To avoid sheltering by Rame Head to the west and near-shore processes, we limit our C_{D10N} observations to a narrower wind sector of 180–220°. Figure 4 shows the relationship between C_{D10N} and $U_{10\mathrm{N}}$ from the Windmaster Pro sonic anemometer. Also shown are the predicted C_{D10N} from the COARE (Coupled Ocean-Atmosphere Response Experiment) model version 3.5 (Edson et al., 2013) and Smith (1980). When the sensors were initially placed at 15 m a.m.s.l., measured C_{D10N} values were significantly higher than the open-ocean parameterisations at moderate wind speeds, probably because land/foreshore was within the flux footprint. At 18 m a.m.s.l., the mean C_{D10N} at intermediate-to-high wind speeds was in close agreement with bulk predictions. Measured C_{D10N} are sometimes elevated at wind speeds less than $\sim 5\,\mathrm{m\,s^{-1}}$, possibly due to increased flow distortion or minor land influence.

At 27 m a.m.s.l., C_{D10N} measurements from the Windmaster Pro within the wind sector of 180–220° are limited (valid flux segments $N = 42$), which appear to be lower than the open-ocean parameterisations by about 0.2×10^{-3}. These low C_{D10N} values may partly be due to remaining uncertainties in the Windmaster Pro sonic anemometer even after applying the bias correction to the w axis. Our coastal mea-

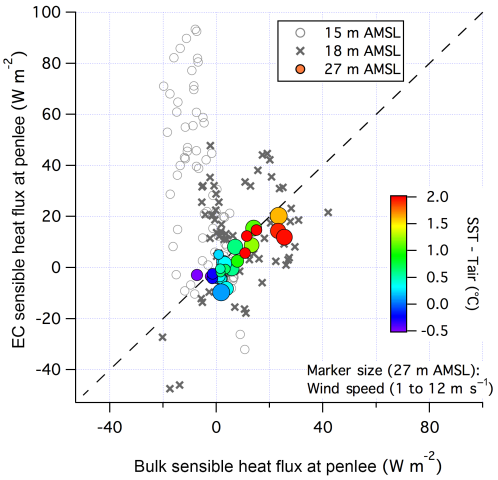

Figure 5. EC sensible heat flux vs. bulk sensible heat flux computed using SST from the L4 station. For June–July 2014 (27 m a.m.s.l.), the colour-coding indicates the sea-air temperature difference, while the marker size corresponds to wind speed (1–12 m s^{-1}).

surements show that at a tilt angle of 5°, the recommended w correction increases u_* from the Windmaster Pro by 6 % (and increases scalar fluxes by 14 %). Relative to the R3 sonic anemometer, this reduces the low bias in the Windmaster Pro u_* from 9–10 to 3–4 %. The remaining 3–4 % bias can account for an approximate 0.1×10^{-3} underestimation of C_{D10N} by the Windmaster Pro.

Figure 5 shows a comparison between the EC sensible heat flux and the bulk sensible heat flux. The latter is computed from SST from the L4 buoy (1 m depth), potential air temperature and U_{10N} from PPAO, and the heat transfer rate from the COARE model (Fairall et al., 2003). Measurement and prediction are not far from the 1 : 1 line at a sampling height of 27 m a.m.s.l. (slope = 0.82; $r^2 = 0.72$). A perfect agreement is not expected here, as any spatial heterogeneity in SST along the 6 km between L4 and PPAO (e.g. due to the Tamar Estuary outflow) or near-surface vertical gradient in seawater temperature would contribute to the discrepancy between measured and predicted sensible heat flux. At the initial sampling height of 15 m a.m.s.l., measured sensible heat flux is often very large and shows no correlation with the bulk flux estimate, most likely due to the terrestrial influence within the flux footprint. At 18 m a.m.s.l., a better coherence is observed but significant scatter remains, probably because the largest horizontal variability in SST is close to shore (and occupies more of the footprint at 18 m than at 27 m). Overall, the comparisons above suggest that the mean measured fluxes at a sampling height $>= 18$ m during south-westerly winds are within 20 % of the expected open-ocean air–sea transfer rates.

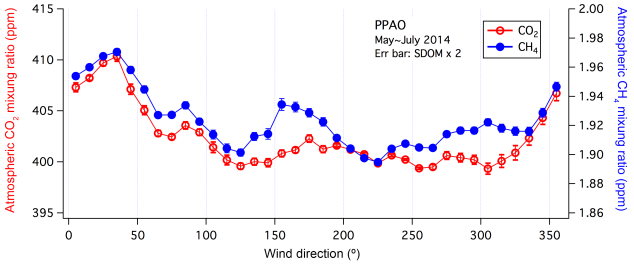

Figure 6. Atmospheric mixing ratios of CO_2 and CH_4 as a function of wind direction. Error bars indicate two standard errors within each wind direction bin. CO_2 and CH_4 mixing ratios were generally lower for south-westerly winds (180–240°) than for northerly wind sectors.

4 Results and discussion

4.1 Variability in CO_2 and CH_4 mixing ratios

Mixing ratios of CO_2, and CH_4 (C_{CO_2} and C_{CH_4}) varied at PPAO depending on wind direction (Fig. 6). On average between May and July 2014, C_{CO_2} and C_{CH_4} were generally higher for winds blowing from land than for winds blowing from the sea, likely due to the much greater terrestrial emissions of these gases and also different boundary layer dynamics. Mean C_{CO_2} and C_{CH_4} from the south-west sector (180–240°) are similar to "well-mixed" atmospheric observations from sites such as Mauna Loa and Mace Head, consistent with the long atmospheric lifetime of these gases. Mean diel cycles in C_{CO_2} and C_{CH_4} between May and July 2014 during onshore (110–240°) and offshore (300–60°) wind flows are shown in Fig. 7. C_{CO_2} and C_{CH_4} for onshore winds show little diel variability, consistent with the relatively small air–sea CO_2 and CH_4 fluxes (on a per area basis). C_{CO_2} and C_{CH_4} for offshore winds increased at night and peaked in the early morning. Night-time wind speeds tend to be low in offshore flow, with an average of ~ 3 m s^{-1} during these months. The resultant low atmospheric turbulence favours the formation of a shallow nocturnal boundary layer, which traps surface emissions. Between about 11:00 and 20:00 UTC, C_{CO_2} was lower for offshore winds than for onshore winds, probably due to terrestrial photosynthesis. Similar diel cycles in C_{CO_2} and C_{CH_4} are often observed at terrestrial sites (e.g. Winderlich et al., 2014). Clear day/night differences were also apparent in the mixing ratios of oxygenated volatile organic compounds measured from the rooftop of PML (Yang et al., 2013). While not the focus of this work, it is worth noting that the elevated atmospheric CO_2 and CH_4 in the early morning will influence their air–sea fluxes in coastal regions during offshore conditions.

4.2 Detection limit of CH_4 flux measurement

In this section, we examine the eddy covariance flux detection limit of CH_4 and its dependence on instrumental noise as

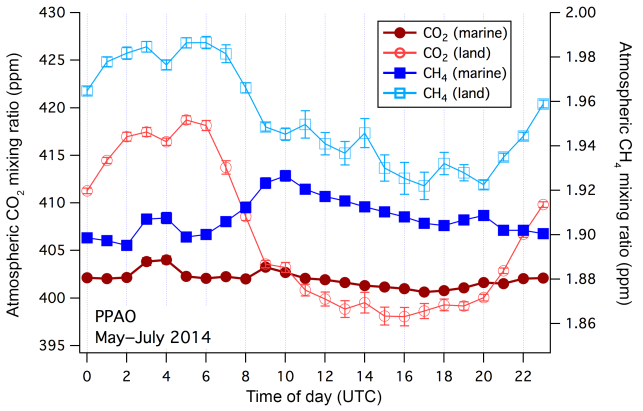

Figure 7. Mean diel cycles in the mixing ratios of CO_2 and CH_4. Error bars indicate two standard errors within each hour bin. Diel variability for both gases is small during onshore flow (marine winds, 110–240°). Mixing ratios of CO_2 and CH_4 during offshore flow (wind from land, 300–60°) increase at night and peak in the early morning.

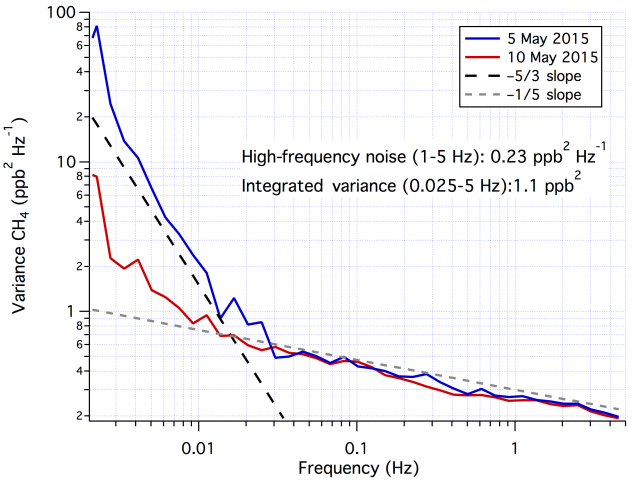

Figure 8. Variance spectra of CH_4 on two days of south-westerly winds. Variance at frequencies above ∼ 0.025 Hz is dominated by noise, while ambient variability accounts for most of the low-frequency variance.

well as ambient variability. Blomquist et al. (2014) estimated an hourly CO_2 flux detection limit of ∼ 1 mmole m^{-2} d^{-1} for a prototype version of the Picarro analyzer (G-1301-f) with a Nafion dryer at a wind speed of 8 m s^{-1} and in a neutral atmosphere. This represents an order of magnitude improvement over previous CO_2 sensors (e.g. Licor) and is lower in magnitude than the typical air–sea CO_2 flux. Based on terrestrial eddy covariance measurements, Peltola et al. (2014) estimated the CH_4 flux detection limit using the Picarro analyzers G-1301-f and G-2311-f to be ∼ 170 µmole m^{-2} d^{-1} for an averaging interval (T) of 30 min (∼ 120 µmole m^{-2} d^{-1} at $T = 60$ min). In comparison, the expected emissions of CH_4 (F_{CH_4}) based on dissolved CH_4 in the open ocean are generally less than 10 µmole m^{-2} d^{-1} (e.g. Forster et al., 2009).

We estimate the air–sea CH_4 flux detection limit using an empirical and a theoretical approach. First, following Spirig et al. (2005), we compute the variability in the $C_{CH_4} : w$ covariance at a time lag far away from the true lag (i.e. +300 s). During periods of consistent south-westerly winds, the 1σ of this null CH_4 flux is 15 µmole m^{-2} d^{-1} at $T = 10$ min. The flux detection limit (defined as 3σ) should thus be 18 µmole m^{-2} d^{-1} ($= 3 \times 15/6^{0.5}$) for an hourly average and 4 µmole m^{-2} d^{-1} for a daily average.

Based on theory and scalar flux observations, Blomquist et al. (2010, 2012) attributed total uncertainty in eddy covariance flux (δF_C) to ambient variance ($\sigma^2_{C_a}$) and sensor noise ($\sigma^2_{C_n}$):

$$\delta F_C = \frac{2\sigma_W}{\sqrt{T}}\left[\sigma^2_{C_a}\tau_{WC} + \sigma^2_{C_n}\tau_{C_n}\right]^{1/2} = \frac{2\sigma_W}{\sqrt{T}}\left[\sigma^2_{C_a}\tau_{WC} + \frac{\varphi_{C_n}}{4}\right]^{1/2}. \quad (1)$$

Here τ_{WC} and τ_{C_n} are the integral timescales for ambient variance and noise variance. The noise term in Eq. (1) relates to φ_{C_n}, the band-limited noise. According to the manufacturer the precision of the Picarro G2311-f is ≤ 3 ppb for CH_4 at a sampling rate of 10 Hz. The variance spectra of CH_4 during two periods of south-westerly winds are shown in Fig. 8. Variance below ∼ 0.025 Hz largely follows the expected −5/3 slope for atmospheric transport. At frequencies above ∼ 0.025 Hz, the Picarro shows a "pink" background noise that approximately scales to a −1/5 slope. The integrated variance from 0.025 to 5 Hz is ∼ 1.1 ppb^2, while the average φ_{C_n} between 1 and 5 Hz is ∼ 0.23 ppb^2 Hz^{-1}. Considering noise alone (i.e. $\sigma^2_{C_a} = 0$), for a neutral atmosphere at a wind speed of 10 m s^{-1} and a sampling height of 20 m a.m.s.l., Eq. (1) predicts an uncertainty in hourly CH_4 flux of 11 µmole m^{-2} d^{-1} (Fig. 9). From the expected air–sea CH_4 flux, using similarity theory we can estimate the variability in C_{CH_4} caused by air–sea exchange in a neutral atmosphere as $3|F_{CH_4}|/u_*$ (e.g. Fairall et al., 2000; Blomquist et al., 2010). For $F_{CH_4} = 2$–20 µmole m^{-2} d^{-1} and $u_* = 0.3$ m s^{-1}, this corresponds to a predicted variability of 0.006–0.057 ppb. Figure 9 shows that if the ambient variability in C_{CH_4} were in this range, the hourly flux uncertainty would be dominated by sensor noise.

The observed ambient variability in C_{CH_4} tends to be more than an order of magnitude greater than is predicted from similarity theory, which is likely related to processes other than air–sea flux (e.g. spatial heterogeneity and horizontal atmospheric transport). We estimate $\sigma^2_{C_a}$ as the second point of the autocovariance of C_{CH_4} (the difference between the first and second points of the autocovariance equates to $\sigma^2_{C_n}$ of ∼ 1 ppb^2). At PPAO, the minimum CH_4 ambient variability during onshore flow is 0.2 ppb ($\sigma^2_{C_a} = 0.04$ ppb^2),

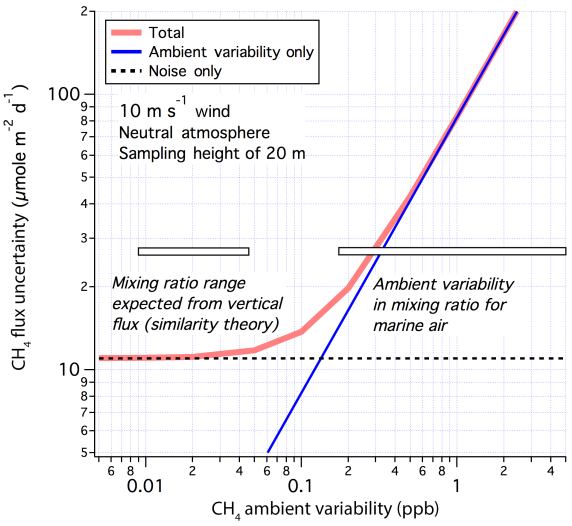

Figure 9. Estimated uncertainty in hourly averaged EC flux of CH_4. Typical observed and predicted (based on similarity theory for the open ocean) values of the ambient variability in CH_4 mixing ratio are shown by the horizontal bars.

which corresponds to a predicted hourly flux uncertainty of 20 µmole m^{-2} d^{-1} (Fig. 9). This is close to our empirical estimate of the CH_4 flux detection limit above. With increasing σ_{C_a} (i.e. more variable C_{CH_4}), the flux uncertainty increases substantially and becomes much greater than F_{CH_4}, while the relative importance of $\sigma^2_{C_n}$ decreases. Thus, we expect the 10-fold greater CH_4 flux detection limit estimated by Peltola et al. (2014) to be due to the higher variability in C_{CH_4} over land than at our marine site (for onshore winds only). Over the open ocean where σ_{C_a} in CH_4 is likely to be even lower than at PPAO, the flux detection limit for CH_4 should slightly decrease.

From the analysis above, it seems that an improvement in the precision of the CH_4 instrument will only marginally reduce the uncertainty in CH_4 flux. Blomquist et al. (2010) arrived at a similar conclusion in an analysis of air–sea carbon monoxide flux. At present, the relative CH_4 flux uncertainty is best minimised by measuring in regions of large flux (i.e. high seawater supersaturation and strong winds) and minimal ambient variability (i.e. spatially homogenous environment).

Blomquist et al. (2010) and Yang et al. (2011) estimated the high-frequency loss in dimethylsulfide flux of typically less than 5 % from the same type of Nafion dryer as used in this study. Flux attenuation by the tubing itself should be negligible given the turbulent flow. Considering the other larger random uncertainties in our CO_2 and CH_4 fluxes, we present the measured fluxes without any attenuation correction in this paper.

4.3 CO_2 flux

Air–sea CO_2 fluxes measured at sampling height of 27 m a.m.s.l. between June and July 2014 were generally small (Fig. 10). Diurnal land–sea breezes were common and durations of onshore winds tended to be short during this period. CO_2 fluxes from the south-west (negative = into the ocean) ranged between 3 and −9 mmole m^{-2} d^{-1} (mean of −3 mmole m^{-2} d^{-1}) during the relatively windy periods on 27 June and 4 July. Seawater pCO_2 at the L4 station ranged between 326 and 345 µatm (mean of 337 µatm) from 9 June to 7 July 2014. The atmospheric CO_2 mixing ratio at L4 agrees well with Picarro measurements at PPAO during onshore flow (Fig. 10). Using the air–sea difference in partial pressure of CO_2 (ΔpCO_2), SST and salinity at L4, as well as wind speed at PPAO, we compute the expected air–sea CO_2 flux as $k_W \cdot \alpha \cdot \Delta pCO_2$, where α is the solubility of CO_2 and k_W is the gas transfer velocity from Nightingale et al. (2000) adjusted for Schmidt number. The expected air–sea CO_2 flux of −1 to −5 mmole m^{-2} d^{-1} (mean of −3 mmole m^{-2} d^{-1}) on 27 June and 4 July are of the same magnitude as our EC measurements. The mean EC CO_2 flux could not be distinguished from zero in the second half of July, consistent with the increase in seawater pCO_2 at L4. The spring algal bloom ended abruptly in early July 2014, with chlorophyll *a* concentration dropping from ∼ 3 to less than 1 mg m^{-3} (http://www.westernchannelobservatory.org.uk/buoys.php). The rapid warming of seawater from ∼ 13 °C in June to ∼ 18 °C in July aided a rapid approach towards air–sea CO_2 equilibrium by the middle of July 2014.

Air-to-sea CO_2 fluxes as substantial as −90 mmole m^{-2} d^{-1} were observed between April and June 2015 (sampling height of 18 m a.m.s.l., Fig. 11). For the south-west sector, the mean fluxes (standard errors) computed from the Windmaster Pro and the R3 sonic anemometers were −19.3(±1.4) and −23.7(±1.4) mmole m^{-2} d^{-1} respectively during this period. The reduced mean flux from the Windmaster Pro was primarily caused by signal dropouts in this anemometer during moderate-to-heavy precipitation, which tended to coincide with high wind speeds (and greater air–sea transfer). When both sonic anemometers were functional, CO_2 fluxes computed from the Windmaster Pro and the R3 demonstrate excellent agreement (slope = 0.98, $r^2 = 0.95$). Example CO_2 cospectra over about half a day from 24 April (wind speed of 8 m s^{-1}) and 10 May 2015 (wind speed of 6 m s^{-1}) are shown in Fig. 12. The observed cospectra are fairly well described by theoretical fits for a neutral atmosphere (Kaimal et al., 1972). Minimal (< 10 %) flux loss at high frequencies is evident, as expected. Hourly CO_2 flux (reversed in sign for clarity) during this period clearly increased with wind speed (Fig. 13). Unfortunately seawater pCO_2 was not measured during this period for comparison. For reference, pCO_2 measurements from L4 in May 2014 had a mean (1σ) of 306(26) µatm, implying a ΔpCO_2 close to −100 µatm. We compute the predicted

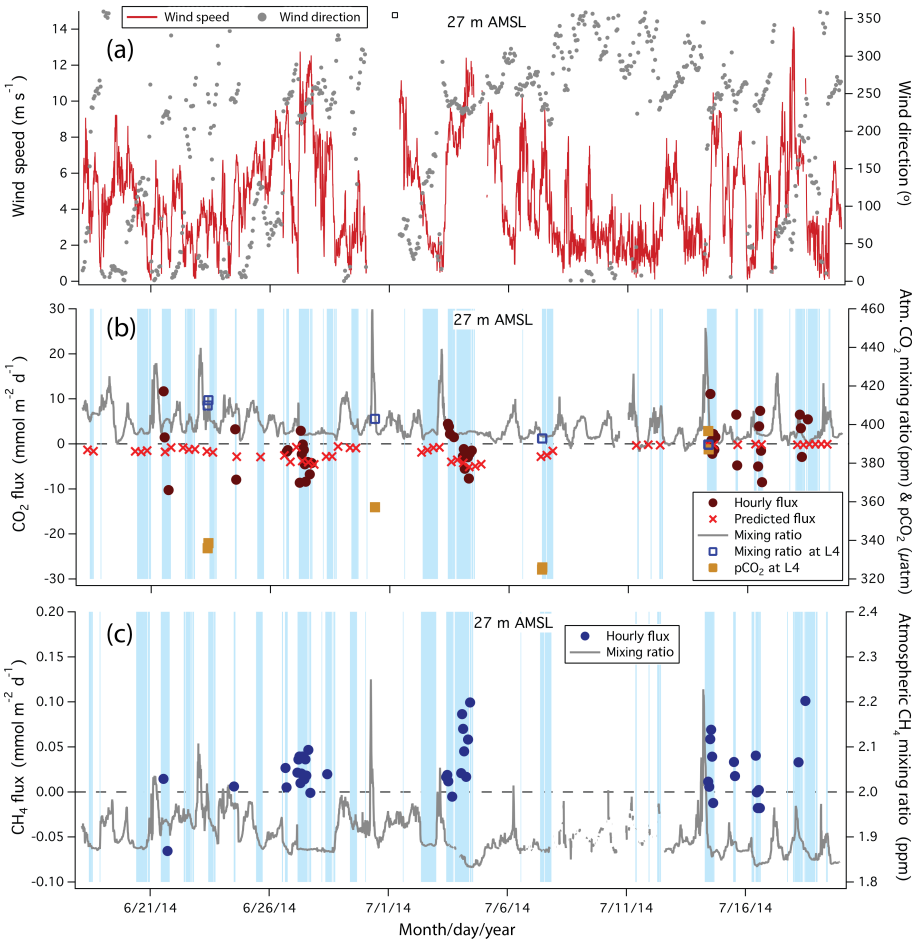

Figure 10. Time series of **(a)** wind speed and direction, **(b)** CO_2 flux and mixing ratio, and **(c)** CH_4 flux and mixing ratio during June–July 2014 (sampling height of 27 m a.m.s.l.). Cyan shading indicates onshore winds. Fluxes are limited to the south-west wind sector only. Also shown are pCO_2 and atmospheric CO_2 mixing ratio from the L4 station. Negative CO_2 fluxes on the order of a few mmole m^{-2} d^{-1} were observed during the windy periods on 27 June and 4 July. By late July, observed CO_2 fluxes were indistinguishable from zero, consistent with near saturation of seawater pCO_2 at the L4 station. CH_4 flux has a positive mean, suggesting sea-to-air emission.

CO_2 fluxes at SST of 12.5 °C (mean from the E1 station) and ΔpCO_2 of −50 and −100 µatm. During most of this period, EC CO_2 flux is fairly close to prediction using $\Delta pCO_2 = -100$ µatm. Towards late May/beginning of June, the magnitude of CO_2 flux appeared to be smaller at high wind speeds. A reduction in ΔpCO_2 as occurred in 2014 could explain the declining CO_2 fluxes in 2015.

Measured CO_2 flux from the south-west between May and June 2014 (sampling height of 15 m a.m.s.l.) varied from a mean (±1 standard error) of about 40(±8) mmole m^{-2} d^{-1} at night to −55(±11) mmole m^{-2} d^{-1} during the day (Fig. 14). Mean wind speeds were fairly similar between day and night at around 5 m s^{-1} during this period. The pronounced diel variability and large magnitude of the CO_2 flux suggest that these fluxes were likely affected by photosynthesis and respiration from land upwind of the observatory building and/or organisms living on the foreshore. As atmosphere–land exchange of CO_2 can be more than an order of magnitude greater than air–sea CO_2 flux on a per area basis (e.g. Goulden et al., 1996), a relatively small terrestrial contribution to the flux footprint (> 5 % spatially) could significantly bias the EC measurement. At sampling heights ≥ 18 m a.m.s.l., CO_2 fluxes show much less diel variation, as would be largely expected for air–sea transfer (Fig. 14). However, the possibility of minor influence from land/foreshore on measurements at 18 m a.m.s.l. cannot be entirely ruled out. Such local effects might explain some of the scatter in CO_2 fluxes at wind speeds below ∼ 5 m s^{-1}, i.e. when the flux footprint was probably closer to land.

Overall, except at the lowest sampling height, air–sea CO_2 fluxes by EC show the expected magnitude and direction in the mean. High resolution CO_2 fluxes demonstrate significant temporal variability, which is often not well captured by the weekly seawater sampling at L4. We plan to make more regular measurements of seawater pCO_2, SST, and salinity within the flux footprint in the future (e.g. as discrete wa-

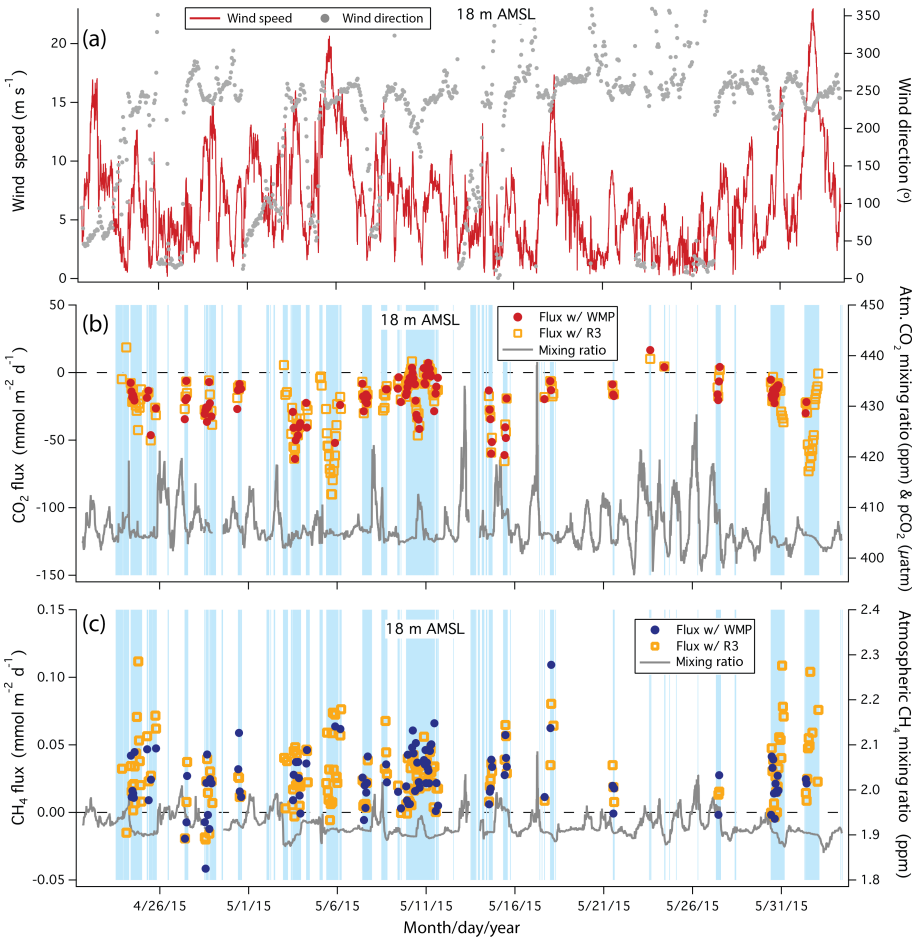

Figure 11. As Fig. 10, but during April–June 2015 (sampling height of 18 m a.m.s.l.). Fluxes were computed from both the Windmaster Pro and the R3 sonic anemometers. Large air-to-sea flux of CO_2 is observed during high wind speed events, while CH_4 flux is almost always positive.

ter samples or using a semi-automated dissolved measurement system on Plymouth Marine Laboratory's research vessel *Quest*), which will enable a direct estimate of the CO_2 gas transfer velocity in a coastal environment.

4.4 CH_4 flux

We use historical observations to assess the validity of the EC CH_4 fluxes since dissolved CH_4 was not measured during 2014–2015. Surface CH_4 saturation values of around 2000 % were measured at the mouth of the Tamar Estuary in spring 2001 by Upstill-Goddard and Barnes (2016). At a SST of 10 °C and wind speed of 10 m s^{-1}, CH_4 saturation of 2000 % implies a predicted CH_4 flux of ~ 0.2 mmol m^{-2} d^{-1} (k_W from Nightingale et al., 2000). Moving further out from the estuary mouth, dissolved CH_4 concentration is expected to decrease due to dilution and oxidation. A strong inverse relationship between CH_4 concentration and salinity has been demonstrated by previous investigators (e.g. Upstill-Goddard et al., 2000), with higher CH_4 concentrations found in fresher waters. According to the compilation by Bange (2006), typical seawater saturations of CH_4 range from 110 to 340 % in the shelf waters of the North Sea, resulting in fluxes on the order of 10 µmole m^{-2} d^{-1}.

Over the three measurement periods presented here, mean EC CH_4 fluxes ranged between 16 and 30 µmole m^{-2} d^{-1} in the south-west wind sector, with peak emissions above ~ 50 µmole m^{-2} d^{-1} (Figs. 10 and 11). As with CO_2, during April–June 2015 the smaller mean CH_4 flux computed from the Windmaster Pro anemometer than from the R3 is primarily due to signal dropouts in the former during rainy, windy conditions (Table 1). The cospectra of CH_4 are noisier than those of CO_2 (Fig. 12) but demonstrate the expected spectral shape. The lowest mean CH_4 fluxes were observed at a sampling height of 15 m a.m.s.l., when the flux footprint should be the closest to shore. This suggests that surface waters, rather than the foreshore/land, are the predominant source of CH_4 at PPAO. In other words, the EC CH_4 fluxes during the low mast period in May–June 2014 are likely underestimates of air–sea transfer.

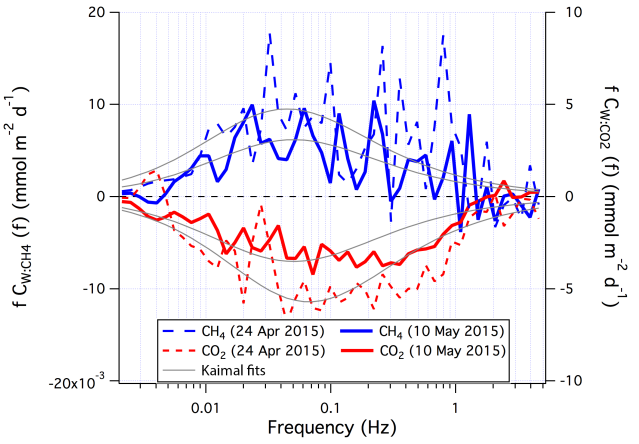

Figure 12. Mean CO_2 and CH_4 cospectra over about half a day for 24 April (wind speed of 8 m s^{-1}) and 10 May 2015 (wind speed of 6 m s^{-1}). Measurements were made at 18 m a.m.s.l. and from the south-westerly direction. Theoretical spectral fits (Kaimal et al., 1972) are also shown.

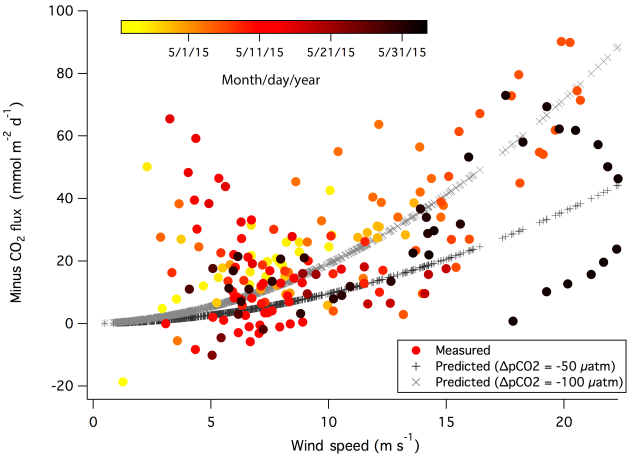

Figure 13. Relationship between CO_2 flux (R3 sonic anemometer; reversed in sign) and wind speed during April–June 2015 (sampling height of 18 m a.m.s.l.). Predicted CO_2 fluxes assuming ΔpCO_2 of -50 and -100 µatm are also shown.

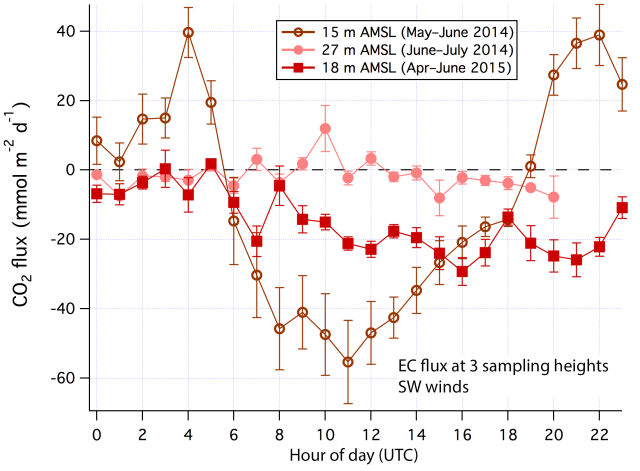

Figure 14. Diel variations in CO_2 fluxes at three sampling heights for south-westerly winds (180–240°). Error bars correspond to standard errors within each hourly bin. At a sampling height of 15 m a.m.s.l., large diel variability in CO_2 flux was observed most likely due to a local, terrestrial influence. Fluxes measured at $\geq$ 18 m a.m.s.l. exhibit much less diel variability.

CH_4 fluxes from the north-east wind sector (the direction of Plymouth Sound) are on average 2–3 times higher than fluxes from the south-west (Fig. 15), suggesting higher CH_4 concentrations in the Tamar Estuary outflow than in open water. CH_4 fluxes from the south-west show a significant but weak relationship with wind speed ($r = 0.33$ during June–July 2014; $r = 0.25$ during April–June 2015; $p < 0.05$). The weak relationship between CH_4 flux and wind speed was likely in part due to variable seawater CH_4 concentrations. CH_4 emissions do not obviously vary with time of day but they tend to be higher during incoming (rising) tide than during outgoing (falling) tide. In Fig. 16, CH_4 fluxes from the south-westerly direction (April–June 2015) are plotted against hours after low water (low tide occurs at hour zero; high tide occurs near hour six). The median, 25, and 75 % percentiles within each hour bin are also shown. The largest average CH_4 emissions are observed in the first $\sim$ 4 h after low tide, while CH_4 fluxes during the falling tide are lower and less variable. Mean CH_4 fluxes were also $\sim$ 50 % higher during spring tide (here limited to daily tidal amplitude $>$ 4 m) than during neap tide (daily tidal amplitude $<$ 3 m). These patterns are consistent with an incoming tidal current that pushes the CH_4-rich surface outflow from the Tamar Estuary around the Rame peninsula (Uncles et al., 2015).

To further examine the influence of the Tamar estuarine plume, a 3-dimensional hydrodynamic Finite Volume Community Ocean Model (FVCOM, Chen et al., 2003) was run for April–June 2011 with tidal forcing at the boundaries (TPXO, Egbert et al., 2010), surface wind (Met Office Unified Model, Davies et al., 2005), surface heating (NCEP Reanalysis-2, Kanamitsu et al., 2002), and river input (E-HYPE, Donnelly et al., 2012) at variable resolution (15 km at the open boundaries near the shelf edge and 150 m near the Plymouth Sound). The model predicts that within 1 km south-south-west of Penlee, surface layer ($\sim$ 0.2 m thick) salinity tends to be lower during rising tide (about 33.4–33.7) than during falling tide (about 33.9–34.1). This suggests a greater freshwater influence from the Tamar at the surface during rising tide, qualitatively consistent with our CH_4 flux observations. Natural processes other than direct air–sea gas transfer (e.g. ebullition) could also contribute to the variability in CH_4 fluxes. Quantifications of the temporal/spatial seawater CH_4 distribution within the PPAO flux footprint and

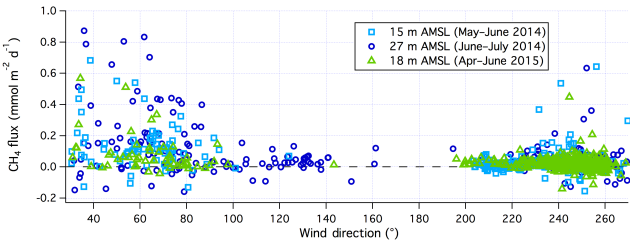

Figure 15. Hourly CH_4 flux as a function of wind direction at all three sampling heights. Larger CH_4 emissions are generally observed when winds are from the north-east (direction of Plymouth Sound) compared to from the south-west (open water), likely due to elevated seawater CH_4 concentrations in the estuarine outflow.

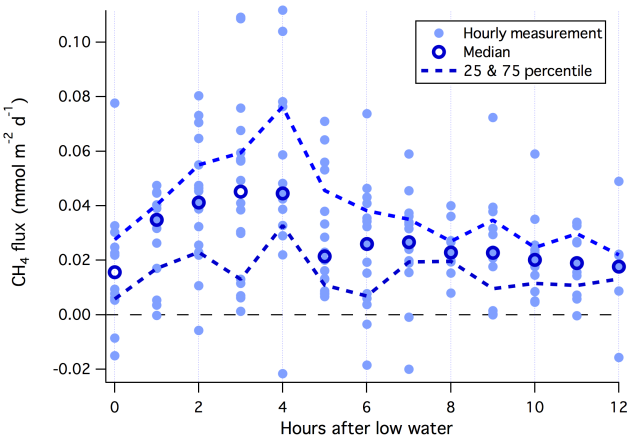

Figure 16. Hourly CH_4 flux from the south-west wind sector (R3 sonic anemometer) vs. hours after low water (18 m a.m.s.l.). Elevated CH_4 emissions are observed in the first $\sim$4 h after low tide, consistent with an enhanced source of CH_4 in the Tamar estuarine outflow driven by the local tidal circulation.

measurements of the pelagic/benthic cycling of CH_4 is essential for addressing this uncertainty.

CH_4 emissions of a few tens of µmole m^{-2} d^{-1} at PPAO are higher than estimates for the open ocean (e.g. Forster et al., 2009) and are lower than previous measurements over other aquatic systems. Kitidis et al. (2007) measured a CH_4 emission of 63 µmole m^{-2} d^{-1} using a floating chamber in the Ria de Vigo (a large coastal embayment), consistent with wind-driven turbulent diffusivity models for the conditions at the time of the chamber deployment. These authors also estimated fluxes up to 170 µmole m^{-2} d^{-1} during periods when the chamber was not deployed. With an open path sensor Podgrajsek et al. (2014) recently measured CH_4 emissions from a Swedish lake using the EC technique. Lake CH_4 emissions range from near zero during the day to over 20 mmole m^{-2} d^{-1} at night (3 orders of magnitude higher than observations at PPAO). Aircraft mixing ratio measurements suggest that CH_4 emissions from the partially ice-covered Arctic are 4–5 times larger than mean emissions at PPAO (Kort et al., 2012). Our observations and estimates of the CH_4 flux uncertainty suggest that an EC system such as the one employed here should be able to quantify emissions from those CH_4 hotspots.

5 Conclusions

Air–sea fluxes of CO_2, CH_4, momentum, and sensible heat were measured by the EC technique in 2014 and 2015 from the Penlee Point Atmospheric Observatory (PPAO) on the south-west coast of the UK. Observed momentum and sensible heat transfer from the south-west wind sector are in the mean within ±20 % of the bulk transfer estimates at a sampling height of $\geq$ 18 m a.m.s.l., which makes PPAO a suitable site for long-term, high temporal resolution measurements of air–sea exchange in shelf regions.

Air–sea CO_2 fluxes demonstrate a positive dependence on wind speed and a rapid decline in magnitude from late spring to early summer in both 2014 and 2015, coinciding with reduced air–sea ΔpCO_2 driven by the demise of the spring algal bloom and the seasonal warming of the sea. We report the first successful EC flux measurements of CH_4 from the marine environment. The CH_4 flux detection limit is estimated to be 20 µmole m^{-2} d^{-1} for an hourly average (4 µmole m^{-2} d^{-1} for a daily average), which is valuable information for planning future open-ocean applications of this technique. Uncertainty in CH_4 fluxes is largely due to ambient variability in atmospheric CH_4 mixing ratio rather than due to instrumental noise. Observed CH_4 emissions are on the order of tens of µmole m^{-2} d^{-1}; a reasonable magnitude for an estuarine-influenced coastal region. CH_4 fluxes are generally higher when the wind is from the Plymouth Sound than when the wind is from the open water sector. Furthermore CH_4 emissions from the open water are greater during rising tide than during falling tide, implying a source of CH_4 in the estuarine outflow that is affected by the local tidal circulation.

Appendix A: Quality control on eddy covariance fluxes

Conservative quality control criteria computed from 10 min flux averaging intervals are used to remove flux measurements during unfavourable conditions (Table A1). Periods of highly variable wind direction ($\sigma > 10°$) and positive momentum flux are discarded on the basis of non-stationarity, which tends to occur during calm conditions or the passage of a weather front. We also reject fluxes that do not pass the statistical quality control tests for skewness and kurtosis of w and integral turbulence characteristics of $\overline{u'w'}$ (Foken and Wichura, 1996; Vickers and Mahrt, 1997). Averaged valid momentum cospectra and normalized Ogives (Oncley, 1989) on 3, 5, and 10 May 2015 (R3 sonic anemometer) are shown in Fig. A1. Mean wind speeds were 12, 17, and 6 m s^{-1} on these three days. The Ogives approached zero at 0.0017 Hz and approached one at 5 Hz, indicating that the 10 min averaging interval captured the majority of the turbulent flux.

To minimise the impact of horizontal transport on CO_2 and CH_4 fluxes, we set thresholds defined by the ranges and trends in mixing ratios (C_{CO_2} and C_{CH_4}) as well as the horizontal fluxes of these gases. Following Blomquist et al. (2012, 2014), we compute the horizontal fluxes as $\overline{u'C'}$ and $\overline{v'C'}$. Here u and v represent the along-stream and cross-stream wind velocities after double rotation. Large horizontal fluxes suggest excessive spatial heterogeneity/nonstationarity. For CH_4 only, we also eliminate periods when the total variance ($= \sigma^2_{C_n} + \sigma^2_{C_a}$) exceeds 2 ppb^2. Since $\sigma^2_{C_n}$ is ~ 1 ppb^2 (see Sect. 4.2), this equates to a σ_{C_a} threshold of $(2\,\text{ppb}^2 - 1\,\text{ppb}^2)^{0.5} = 1$ ppb and an hourly flux uncertainty of ~ 80 µmole m^{-2} d^{-1} (Fig. 9). We note that this σ_{C_a} threshold is almost two orders of magnitude greater than the expected ambient variability in C_{CH_4} due to air–sea flux.

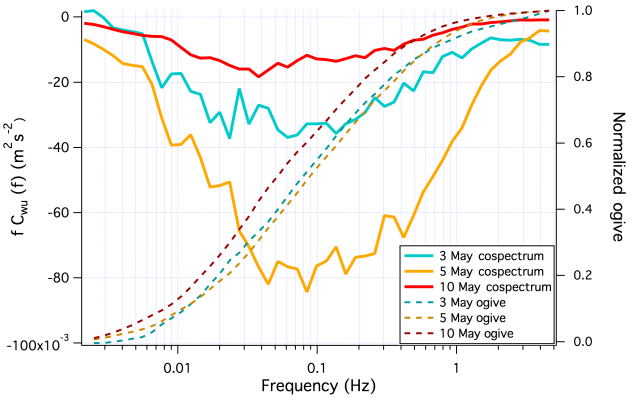

Figure A1. Mean momentum cospectra and normalized Ogives on 3, 5, and 10 May 2015 (R3 sonic anemometer). Mean wind speeds were 12, 17, and 6 m s^{-1} on these three days.

Both sonic anemometers show elevated noise at frequencies above 1 Hz when the relative humidity is near 100 %, likely because of rain and sea spray. For computations of momentum and heat transfer, we remove moisture-related artefacts by simply discarding fluxes when the relative humidity exceeds 95 %. Noise in the sonic anemometer above 1 Hz shows little correlation with C_{CO_2} and C_{CH_4}, such that high humidity does not noticeably affect CO_2 and CH_4 fluxes.

Table A1. Filtering criteria (within 10 min averaging intervals) for quality control of eddy covariance fluxes. These criteria are shown for the south-west air sector only (180° < Wind direction < 240°). The right column indicates the percentage of valid flux data that satisfy the filtering criteria by each stage of the quality control sequence.

	Criteria	Purpose	Percentage passed
Wind	σ in wind direction < 10°	Choose constant wind direction	93
	Negative momentum flux	Check wind profile	92
	Pass skewness, kurtosis, and integral turbulence characteristics tests	Satisfy stationarity of wind	88
CO_2 and CH_4	No gap in Picarro data	Verify Picarro data	92
	Valid wind	Verify physical flux	81
CO_2 only	C_{CO_2} Range < 5 ppm	Satisfy stationarity of CO_2	79
	$\lvert C_{CO_2}$ Trend$\rvert$ < 10 ppm h^{-1}	Satisfy stationarity of CO_2	75
	$\lvert$Horizontal flux$\rvert$ < 500 mmole m^{-2} d^{-1}	Satisfy stationarity of CO_2	74
CH_4 only	C_{CH_4} Range < 20 ppb	Satisfy stationarity of CH_4	80
	$\lvert C_{CH_4}$ Trend$\rvert$ < 20 ppb h^{-1}	Satisfy stationarity of CH_4	75
	Total variance < 2 ppb^2	Reduce flux uncertainty	74
	$\lvert$Horizontal flux$\rvert$ < 0.4 mmole m^{-2} d^{-1}	Satisfy stationarity of CH_4	72
C_{D10N} and sensible heat	180° < Wind direction < 220°	Choose least sheltered wind sector	72
	Relative humidity < 95 %	Remove moisture-related noise	67

Appendix B: Theoretical flux footprint

We use a theoretical flux footprint model (Kljun et al., 2004) to evaluate the suitability of PPAO for air–sea flux measurements. Typical values for south-westerly conditions (i.e. clean marine air) are used in the flux footprint calculations: roughness length (z_0) = 0.0001 m, friction velocity (u_*) = 0.20 m s^{-1}, and standard deviations in w (σ_W) = 0.35, 0.26, 0.18 m s^{-1} (to represent unstable, neutral, stable atmospheres). At a sampling height of 27 m a.m.s.l. (fully raised mast), the predicted upwind distance of maximum flux contribution (X_{max}) is 600–1000 m and the distance of 90 % cumulative flux contribution (X_{90}) is 1500–2600 m (the greater distances correspond to increased stability). For this set up, land/foreshore south-west of the observatory contributes to only 2–3 % (stable) or 3–4 % (neutral/unstable) of the cumulative flux, with the greater contributions corresponding to lower tide. The majority of the flux footprint is over water with a depth of $\sim$ 20 m. Waves are considered to be in deepwater if water depth is greater than half of the wavelength. They start to deviate significantly from deepwater behaviour when the depth is less than about a quarter of the wavelength. At a wind speed of 10 m s^{-1}, fully developed wind waves have a wavelength of $\sim$ 80 m. For wind speeds more than 10 m s^{-1}, wind waves near Penlee could be affected by depth, while swell (which tends to be longer) would almost always be. Thus PPAO should be considered a coastal, rather than a deepwater site.

At moderate-to-high wind speeds, the marine atmosphere is usually near neutral, and the flux footprint tends to be further away from the coastline. Unstable conditions are more likely to occur under low wind speeds, during which the flux footprint shortens and may be more affected by the rocky coastline and near-shore wave breaking. At our minimum sampling height of 15 m a.m.s.l., the predicted X_{max} and X_{90} are 300–500 and 900–1500 m, depending on stability. Land/foreshore south-west of the observatory is still only predicted to account for a small percentage of the cumulative flux (3–6 %, varying with tide and stability). South-east of PPAO where the distance to the water's edge is greater, more terrestrial influence (5–9 %) is expected. We note that the Kljun et al. (2004) flux footprint model is developed for spatially homogeneous environments. A strong point source or sink within the footprint would have a disproportionately large influence on the flux.

Acknowledgements. Trinity House (http://www.trinityhouse.co.uk/) owns the Penlee site and has kindly agreed to rent the building to PML so that instrumentation can be protected from the elements. We are able to access the site thanks to the cooperation of Mount Edgcumbe Estate (http://www.mountedgcumbe.gov.uk/). R. McKay (Gill) advised on the operation and calibration of the Windmaster Pro sonic anemometer. Thanks also to J. Stephens, J. Jury, K. Perrett, A. Staff, and B. Carlton at the Plymouth Marine Laboratory (PML) for their efforts in setting up the site and establishing data communication. R. Torres (PML) helped with the FVCOM model and interpretation of the tidal data. B. Blomquist (NOAA) offered valuable advice on the set-up of Picarro instrument.

Edited by: T. Karl

References

Bange, H. W.: Nitrous oxide and methane in European coastal waters, Estuar. Coast. Shelf Sc., 70, 361–374, 2006.

Bange, H. W., Bartell, U. H., Rapsomanikis, S., and Andreae, M. O.: Methane in the Baltic and North Seas and a reassessment of the marine emissions of methane, Global Biogeochem. Cy., 8, 465–480, 1994.

Bates, T. S., Kelly, K. C., Johnson, J. E., and Gammon, R. H.: A reevaluation of the open ocean source of methane to the atmosphere, J. Geophys. Res., 101, 6953–6961, 1996.

Bell, T. G., De Bruyn, W., Miller, S. D., Ward, B., Christensen, K. H., and Saltzman, E. S.: Air–sea dimethylsulfide (DMS) gas transfer in the North Atlantic: evidence for limited interfacial gas exchange at high wind speed, Atmos. Chem. Phys., 13, 11073–11087, doi:10.5194/acp-13-11073-2013, 2013.

Blomquist, B., Fairall, C. W., Huebert, B. J., Kieber, D., and Westby G.: DMS sea–air transfer velocity: Direct measurements by eddy covariance and parameterization based on the NOAA/COARE gas transfer model, Geophys. Res. Lett., 33, L07601, doi:10.1029/2006GL025735, 2006.

Blomquist, B. W., Huebert, B. J., Fairall, C. W., and Faloona, I. C.: Determining the sea–air flux of dimethylsulfide by eddy correlation using mass spectrometry, Atmos. Meas. Tech., 3, 1–20, doi:10.5194/amt-3-1-2010, 2010.

Blomquist, B. W., Fairall, C. W., Huebert, B. J., and Wilson, S. T.: Direct measurement of the oceanic carbon monoxide flux by eddy correlation, Atmos. Meas. Tech., 5, 3069–3075, doi:10.5194/amt-5-3069-2012, 2012.

Blomquist, B. W., Huebert, B. J., Fairall, C. W., Bariteau, L., Edson, J. B., Hare, J. E., and McGillis, W. R.: Advances in Air-Sea CO_2 Flux Measurement by Eddy Correlation, Bound.-Lay. Meteorol., 152, 245–276, doi:10.1007/s10546-014-9926-2, 2014.

Businger, J. A.: A note on the Businger–Dyer profiles, Bound.-Lay. Meteorol., 42, 145–151, doi:10.1007/978-94-009-2935-7_11, 1988.

Canadell, J. G., Le Quéré, C., Raupach, M. R., Field, C. B., Buitenhuis, E. T., Ciais, P., Conway, T. J., Gillett, N. P., Houghton, R. A., and Marland, G.: Contributions to accelerating atmospheric CO_2 growth from economic activity, carbon intensity, and efficiency of natural sinks, P. Natl. Acad. Sci. USA, 104, 18866–18870, doi:10.1073/pnas.0702737104, 2007.

Chen, C., Liu, H., and Beardsley, R. C.: An Unstructured Grid, Finite-Volume, Three-Dimensional, Primitive Equations Ocean Model: Application to Coastal Ocean and Estuaries, J. Atmos. Ocean. Tech., 20, 159–186, doi:10.1029/2007JC004557, 2003.

Chen, C.-T. A., Huang, T.-H., Chen, Y.-C., Bai, Y., He, X., and Kang, Y.: Air–sea exchanges of CO_2 in the world's coastal seas, Biogeosciences, 10, 6509–6544, doi:10.5194/bg-10-6509-2013, 2013.

Davies, T., Cullen, M. J. P., Malcolm, A. J., Mawson, M. H., Staniforth, A., White, A. A., and Wood, N.: A New Dynamical Core for the Met Office's Global and Regional Modelling of the Atmosphere, Q. J. Roy. Meteor. Soc., 131, 1759–1782, doi:10.1256/qj.04.101, 2005.

Dimitrov, L.: Contribution to atmospheric methane by natural seepages on the Bulgarian continental shelf, Cont. Shelf Res., 22, 2429–2442, 2002.

Donnelly, C., Rosberg, J., and Isberg, K.: A Validation of River Routing Networks for Catchment Modelling from Small to Large Scales, Hydrol. Res., 44, 917–925, doi:10.2166/nh.2012.341, 2012.

Edson, J. B., DeGrandpre, M. D., Frew, N., and McGillis, W. R.: Investigations of air–sea gas exchange in the CoOP coastal air–sea chemical flux program, Oceanography, 21, 34–45, 2008.

Edson, J. B., Jampana, V., Weller, R. A., Bigorre, S. P., Plueddemann, A. J., Fairall, C. W., Miller, S. D., Mahrt, L., Vickers, D., and Hersbach H.: On the exchange of momentum over the open ocean, J. Phys. Oceanogr., 43, 1589–1610, doi:10.1175/JPO-D-12-0173.1, 2013.

Egbert, G. D., Erofeeva, S. Y., and Ray, R. D.: Assimilation of Altimetry Data for Nonlinear Shallow-Water Tides: Quarter-Diurnal Tides of the Northwest European Shelf, Cont. Shelf Res., 30, 668–679, doi:10.1016/j.csr.2009.10.011, 2010.

Fairall, C. W., Hare, J. E., Edson, J. B., and McGillis, W.: Parameterization and micrometeorological measurements of air-sea gas transfer, Bound. Lay. Meteorol., 96, 63–105, 2000.

Fairall, C. W., Bradley, E. F., Hare, J. E., Grachev, A. A., and Edson, J. B.: Bulk parameterization of air-sea fluxes: updates and verification for the COARE algorithm, J. Climate, 16, 571–591, 2003.

Foken, T. and Wichura, B.: Tools for quality assessment of surface-based flux measurements 1, Agr. Forest Meteorol., 78, 83–105, doi:10.1016/0168-1923(95)02248-1, 1996.

Forster, G. L., Upstill-Goddard, R. C., Gist, N., Robinson, R., Uher, G., and Woodward, E. M. S.: Nitrous oxide and methane in the Atlantic Ocean between 501N and 521S: Latitudinal distribution and sea-to-air flux, Deep-Sea Res. Pt. II, 56, 964–976, doi:10.1016/j.dsr2.2008.12.002, 2009.

Goulden, M. L., Munger, J. W., Fan, S.-M., Daube, B. C., and Wofsy, S. C.: Measurements of carbon sequestration by long-term eddy-covariance: Methods and a critical evaluation of accuracy, Glob. Change Biol., 2, 169–182, 1996.

Huebert, B. J., Blomquist, B. W., Hare, J. E., Fairall, C. W., Johnson, J. E., and Bates, T. S.: Measurement of the sea–air DMS flux and transfer velocity using eddy correlation, Geophys. Res. Lett., 31, L23113, doi:10.1029/2004GL021567, 2004.

Hyson, P., Garratt, J. R., and Francey, R. J.: Algebraic and Electronic Corrections of Measured uw Covariance in the Lower Atmosphere, J. Appl. Meteorol., 16, 43–47, 1977.

Kaimal, J. C., Wyngaard, J. C., Izumi, Y., and Cote, O. R.: Spectral characteristics of surface-layer turbulence, Q. J. Roy. Meteor. Soc., 98, 563–589, 1972.

Kanamitsu, M., Ebisuzaki, W., Woollen, J., Yang, S.-K., Hnilo, J. J., Fiorino, M., and Potter, G. L.: NCEP-DOE AMIP-II Reanalysis (R-2), B. Am. Meteorol. Soc., 83, 1631–1643, doi:10.1175/BAMS-83-11-1631, 2002.

Kitidis, V., Tizzard, L., Uher, G., Judd, A., Upstill-Goddard, R. C., Head, I. M., Gray, N. D., Taylor, G., Duran, R., Diez, R., Iglesias, J., and Garcia-Gil, S.: The biogeochemical cycling of methane in Ria de Vigo, NW Spain: Sediment processing and sea-air exchange, J. Marine Syst., 66, 258–271, 2007.

Kitidis, V., Upstill-Goddard, R. C., and Anderson, L. G.: Methane and Nitrous Oxide in surface water along the North-West Passage; Arctic Ocean, Mar. Chem., 121, 80–86, 2010.

Kitidis, V., Hardman-Mountford, N. J., Litt, E., Brown, I., Cummings, D., Hartman, S., Hydes, D., Fishwick, J. R., Harris, C., Martinez-Vicente, V., Malcolm, E., Woodward, S., and Smyth, T. J.: Seasonal dynamics of the carbonate system in the Western English Channel, Cont. Shelf Res., 42, 30–40, 2012.

Kljun, N., Calanca, P., Rotach, M. W., and Schmid, H. P.: A Simple Parameterisation for Flux Footprint Predictions, Bound.-Lay. Meteorol., 112, 503–523, 2004.

Kort, E. A., Wofsy, S. C., Daube, B. C., Diao, M., Elkins, J. W., Gao, R. S., Hintsa, E. J., Hurst, D. F., Jimenez, R., Moore, F. L., Spackman, J. R., and Zondlo, M. A.: Atmospheric observations of Arctic Ocean methane emissions up to 82 degrees north, Nat. Geosci., 5, 318–321, doi:10.1038/ngeo1452, 2012.

Le Quéré, C., Moriarty, R., Andrew, R. M., Peters, G. P., Ciais, P., Friedlingstein, P., Jones, S. D., Sitch, S., Tans, P., Arneth, A., Boden, T. A., Bopp, L., Bozec, Y., Canadell, J. G., Chini, L. P., Chevallier, F., Cosca, C. E., Harris, I., Hoppema, M., Houghton, R. A., House, J. I., Jain, A. K., Johannessen, T., Kato, E., Keeling, R. F., Kitidis, V., Klein Goldewijk, K., Koven, C., Landa, C. S., Landschützer, P., Lenton, A., Lima, I. D., Marland, G., Mathis, J. T., Metzl, N., Nojiri, Y., Olsen, A., Ono, T., Peng, S., Peters, W., Pfeil, B., Poulter, B., Raupach, M. R., Regnier, P., Rödenbeck, C., Saito, S., Salisbury, J. E., Schuster, U., Schwinger, J., Séférian, R., Segschneider, J., Steinhoff, T., Stocker, B. D., Sutton, A. J., Takahashi, T., Tilbrook, B., van der Werf, G. R., Viovy, N., Wang, Y.-P., Wanninkhof, R., Wiltshire, A., and Zeng, N.: Global carbon budget 2014, Earth Syst. Sci. Data, 7, 47–85, doi:10.5194/essd-7-47-2015, 2015.

Lelieveld, J., Crutzen, P. J., and Dentener, F. J.: Changing concentration, lifetime and climate forcing of atmospheric methane, Tellus B, 50, 128–150, 1998.

Manning, A. C. and Keeling, R. F.: Global oceanic and land biotic carbon sinks from the Scripps atmospheric oxygen flask sampling network, Tellus B, 58, 95–116, doi:10.1111/j.1600-0889.2006.00175.x, 2006

McGillis, W. R., Edson, J. B., Hare, J. E., and Fairall, C. W.: Direct covariance air-sea CO_2 fluxes, J. Geophys. Res., 106, 16729–16745, 2001.

Middelburg, J. J., Nieuwenhuize, J., Iversen, N., Høgh, N., De Wilde, H., Helder, W., Seifert, R., and Christof, O.: Methane distribution in European tidal estuaries, Biogeochemistry, 59, 95–119, 2002.

Miller, S. D., Marandino, C., and Saltzman, E. S.: Ship-based measurement of air-sea CO_2 exchange by eddy covariance, J. Geophys. Res., 115, D02304, doi:10.1029/2009JD012193, 2010.

Muller-Karger, F. E., Varela, R., Thunell, R., Luerssen, R., Hu, C., and Walsh, J. J.: The importance of continental margins in the global carbon cycle, Geophys. Res. Lett., 32, L01602, doi:10.1029/2004GL021346, 2005.

Nightingale, P. D., Malin, G, Law, C. S., Watson, A. J., Liss, P. S., Liddicoat, M. I., Boutin, J., and Upstill-Goddard, R. C.: In situ evaluation of air–sea gas exchange parameterizations using novel conservative and volatile tracers, Global Biogeochem. Cy., 14, 373–387, 2000.

Oncley, S. P.: Flux Parameterisation Techniques in the Atmospheric Surface Layer, PhD thesis, 202 pp., Univ. of California, Irvine, 1989.

Peltola, O., Hensen, A., Helfter, C., Belelli Marchesini, L., Bosveld, F. C., van den Bulk, W. C. M., Elbers, J. A., Haapanala, S., Holst, J., Laurila, T., Lindroth, A., Nemitz, E., Röckmann, T., Vermeulen, A. T., and Mammarella, I.: Evaluating the performance of commonly used gas analysers for methane eddy covariance flux measurements: the InGOS inter-comparison field experiment, Biogeosciences, 11, 3163–3186, doi:10.5194/bg-11-3163-2014, 2014.

Podgrajsek, E., Sahlée, E., and Rutgersson A.: Diurnal cycle of lake methane flux, J. Geophys. Res.-Biogeo., 119, 236–248, doi:10.1002/2013JG002327, 2014.

Rella, C.: Accurate Greenhouse Gas Measurements in Humid Gas Streams Using the Picarro G1301 Carbon Dioxide/Methane/Water Vapor Gas Analyzer. White Paper from Picarro INC., 480 Oakmead Parkway, Sunnyvale, CA 94085, 2010.

Shakhova, N., Semiletov, I., Salyuk, A., Yusupov, V., Kosmach, D., and Gustafsson, O.: Extensive methane venting to the atmosphere from sediments of the east Siberian Arctic shelf, Science, 327, 1246–1250, 2010.

Smith, S.: Wind stress and heat flux over the ocean in gale force winds, J. Phys. Oceanogr., 10, 709–726, 1980.

Spirig, C., Neftel, A., Ammann, C., Dommen, J., Grabmer, W., Thielmann, A., Schaub, A., Beauchamp, J., Wisthaler, A., and Hansel, A.: Eddy covariance flux measurements of biogenic VOCs during ECHO 2003 using proton transfer reaction mass spectrometry, Atmos. Chem. Phys., 5, 465–481, doi:10.5194/acp-5-465-2005, 2005.

Sweeney, C., Gloor, E., Jacobson, A. R., Key, R. M., McKinley, G., Sarmiento, J. L., and Wanninkhof, R.: Constraining global air–sea gas exchange for CO_2 with recent bomb ^{14}C measurements, Global Biogeochem. Cy., 21, GB2015, doi:10.1029/2006GB002784, 2007.

Tanner, C. B. and Thurtell, G. W.: Anemoclinometer Measurements of Reynolds Stress and Heat Transport in the Atmospheric Surface Layer, University of Wisconsin Tech. Rep., ECOM-66-G22-F, 82 pp., 1969.

Thomas, H., Bozec, Y., Elkalay, K., and de Baar, H. J. W.: Enhanced open ocean storage of CO_2 from shelf sea pumping, Science, 304, 1005–1008, 2004.

Uncles, R. J., Stephens, J. A., and Harris, C.: Physical processes in a coupled bay-estuary coastal system: Whitesand Bay and Plymouth Sound, Prog. Oceanogr., 137, 360–384, doi:10.1016/j.pocean.2015.04.019, 2015.

Upstill-Goddard, R. C.: Air-sea gas exchange in the coastal zone, Estuar. Coast. Shelf Sc., 70, 388–404, 2006.

Upstill-Goddard, R. C. and Barnes, J.: Methane emissions from UK estuaries: Re-evaluating the estuarine source of tropospheric methane from Europe, Mar. Chem., 180, 14–23, doi:10.1016/j.marchem.2016.01.010, 2016.

Upstill-Goddard, R. C., Barnes, J., Frost, T., Punshon, S., and Owens, N. J. P.: Methane in the southern North Sea: low-salinity inputs, estuarine removal, and atmospheric flux, Global Biogeochem. Cy., 14, 1205–1217, 2000.

Vickers, D. and Mahrt, L.: Quality control and flux sampling problems for tower and aircraft data, J. Atmos. Ocean. Tech., 14, 512–526, doi:10.1175/1520-0426(1997)014<0512:QCAFSP>2.0.CO;2, 1997.

Winderlich, J., Gerbig, C., Kolle, O., and Heimann, M.: Inferences from CO_2 and CH_4 concentration profiles at the Zotino Tall Tower Observatory (ZOTTO) on regional summertime ecosystem fluxes, Biogeosciences, 11, 2055–2068, doi:10.5194/bg-11-2055-2014, 2014.

Yang, M., Blomquist, B. W., Fairall, C. W., Archer, S. D., and Huebert, B. J.: Air-sea exchange of dimethylsulfide in the Southern Ocean: Measurements from SO GasEx compared to temperate and tropical regions, J. Geophys. Res., 116, C00F05, doi:10.1029/2010JC006526, 2011.

Yang, M., Beale, R., Smyth, T., and Blomquist, B.: Measurements of OVOC fluxes by eddy covariance using a proton-transfer-reaction mass spectrometer – method development at a coastal site, Atmos. Chem. Phys., 13, 6165–6184, doi:10.5194/acp-13-6165-2013, 2013.

Yang, M., Bell, T. G., Hopkins, F. E., and Smyth, T. J.: Attribution of atmospheric sulfur dioxide over the English Channel to dimethyl sulfide and changing ship emissions, Atmos. Chem. Phys., 16, 4771–4783, doi:10.5194/acp-16-4771-2016, 2016.

Webb, E. K., Pearman, G. I., and Leuning, R.: Correction of flux measurements for density effects due to heat and water vapour transfer, Q. J. Roy. Meteor., 106, 85–100, 1980.